Nano-Micro Letters

ISSN 2311-6706
e-ISSN 2150-5551
CN 31-2103/TB

ARTICLE

https://doi.org/10.1007/s40820-022-00815-7

Cite as
Nano-Micro Lett.
(2022) 14:79

Received: 23 December 2021
Accepted: 28 January 2022
Published online: 25 March 2022

Fully Roll-to-Roll Processed Efficient Perovskite Solar Cells via Precise Control on the Morphology of PbI_2:CsI Layer

Hengyue Li[1,2], Chuantian Zuo[2], Dechan Angmo[2], Hasitha Weerasinghe[2], Mei Gao[2] ✉, Junliang Yang[1] ✉

HIGHLIGHTS

- The slot-die-coated porous PbI_2:CsI film assisted with nitrogen blowing can promote the rapid and complete transformation of perovskite film.
- The crystallinity and morphology of slot-die-coated perovskite film are significantly improved by controlling substrate temperature.
- Fully slot-die-coated perovskite solar cells achieve a power conversion efficiency (PCE) of 18.13%, and fully roll-to-roll printed flexible PSCs achieve a PCE of 13.00% in ambient condition.

ABSTRACT Perovskite solar cells (PSCs) have attracted tremendous attention as a promising alternative candidate for clean energy generation. Many attempts have been made with various deposition techniques to scale-up manufacturing. Slot-die coating is a robust and facile deposition technique that can be applied in large-area roll-to-roll (R2R) fabrication of thin film solar cells with the advantages of high material utilization, low cost and high throughput. Herein, we demonstrate the encouraging result of PSCs prepared by slot-die coating under ambient environment using a two-step sequential process whereby PbI_2:CsI is slot-die coated first followed by a subsequent slot-die coating of organic cations containing solution. A porous PbI_2:CsI film can promote the rapid and complete transformation into perovskite film. The crystallinity and morphology of perovskite films are significantly improved by optimizing nitrogen blowing and controlling substrate temperature. A power conversion efficiency (PCE) of 18.13% is achieved, which is promising for PSCs fabricated by two-step fully slot-die-coated devices. Furthermore, PSCs with a 1 cm^2 area yield a champion PCE of 15.10%. Moreover, a PCE of 13.00% is obtained on a flexible substrate by the roll-to-roll (R2R) coating, which is one of the highest reported cells with all layers except for metal electrode fabricated by R2R process under ambient condition.

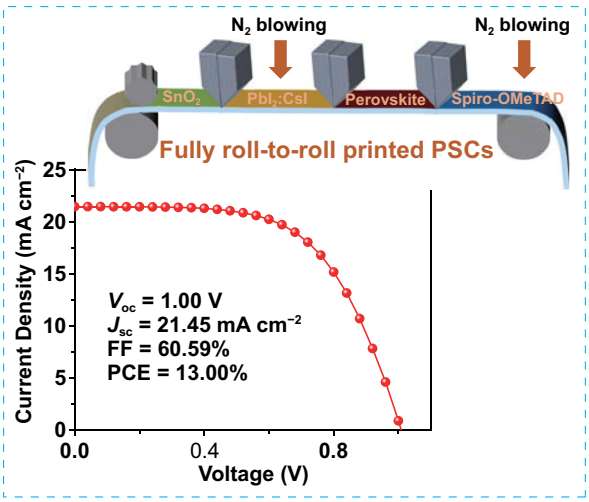

KEYWORDS Perovskite solar cells; Slot-die coating; Roll-to-roll; Ambient condition; Flexible

✉ Mei Gao, mei.gao@csiro.au; Junliang Yang, junliang.yang@csu.edu.cn
[1] Hunan Key Laboratory of Nanophotonics and Devices, School of Physics and Electronics, Central South University, Changsha 410083, People's Republic of China
[2] Flexible Electronics Laboratory, CSIRO Manufacturing, Clayton, VIC 3168, Australia

1 Introduction

The organic–inorganic hybrid perovskite solar cells (PSCs) are considered one of the promising new-generation solar cells. The certified power conversion efficiency (PCE) has reached a remarkable value of 25.7% since the first report in 2009 [1, 2]. These achievements can be attributed to the intrinsic properties of the perovskite material, such as a large absorption coefficient, high charge mobility, low exciton binding energy and low temperature solution processing ability [3–8]. Numerous studies have been attempted to achieve high-quality perovskite films since then, including additives [9–12], solvent engineering [13–15], interface modification [16, 17], and scale-up techniques under ambient fabrication environment [18–22], which would considerably move the development of PSCs to commercialization.

However, most high-performance PSCs are mainly fabricated via spin-coating method due to their accessibility, high repeatability, facile control and suitability for anti-solvent [23, 24]. The major drawback is that spin-coating is unsuitable and difficult to match other scalable printing processes. Recently, growing investigations on PSCs prepared by scalable methods such as blade-coating and slot-die coating have been demonstrated, which are transferable and compatible with the roll-to-roll (R2R) process [25–27]. Among various scalable coating techniques, slot-die coating stands out owing to its high reported PCE, fast coating speeds, high material utilization, and matching with the R2R process [28–30]. It is well known that perovskite film plays an essential role in the performance of PSCs. Both one-step and two-step deposition methods have been broadly employed in the fabrication of PSCs. In one-step perovskite deposition, it is difficult to modulate the crystal growth for forming a uniform film, especially on a large scale [31]. While in the two-step deposition, PbI_2 layer is firstly coated on the substrate by various methods and usually show excellent coverage, which is considered more suitable and reliable for the mass production process. Kim et al. demonstrated a two-step deposition of PSCs with a PCE of 10.9% by fully gravure printing and a PCE of 9.7% by partly R2R process [32]. Later, they adopt tert-butyl alcohol as an anti-solvent to obtain a wide processing window and achieved a PCE of 13.8% for fully R2R processed PSCs [33]. Burkitt et al. used fully R2R process to print p-i-n PSCs with a PCE of 12.2% [34]. Recently, Othman et al. demonstrated that fully R2R slot-die-coated triple-cation PSCs in ambient condition with underlying guanidinium iodide in hole transport layer showed a PCE of 12% [35]. Following the pioneering work by Gratzel group [36], high-performance and stable triple-cation planar heterojunction (PHJ) PSCs have been fabricated successfully via a low temperature sequential solution process [37, 38]. The device with ITO/SnO_2/Perovskite/Spiro-OMeTAD/Ag exhibited a PCE of over 20% by spin coating. Meanwhile, devices can sustain about 80% of the initial PCE when stored in air (humidity = 40%) for over 500 h without any encapsulation. Therefore, if the PSCs fabricated by the scalable method can achieve similar PCEs, especially by R2R coating process, it would tremendously accelerate the commercialization process of PSCs.

In this work, we demonstrate the fabrication of fully slot-die-coated PSCs with a n-i-p structure in ambient condition using a two-step process. All layers of PSC devices were prepared by scalable slot-die coating process except the evaporated metal electrode. The initially formed PbI_2:CsI film showing porous morphology is able to facilitate the fast and complete conversion of PbI_2:CsI film to a pin-hole-free perovskite film which was assisted with heating and N_2 blowing, leading to the fully slot-die-coated PSC devices with a max PCE of 18.13%. Furthermore, devices with a 1 cm^2 area yielded a champion PCE of 15.10%. Remarkably, R2R processed PSC devices achieved a maximum PCE of 13.00%. The results provide significant and continued inspiration for processing high-performance, large-area flexible PSCs, which is helpful for promoting the potential commercialization of PSCs.

2 Experimental Details

2.1 Materials

All of the chemical materials were used directly without any purification, including tin oxide precursor (SnO_2, 15% in H_2O colloidal dispersion, Alfa Aesar), lead iodide (PbI_2, 99%, Greatcell Solar), cesium iodide (CsI, 99%, Strem Chemicals, inc.), formamidinium iodide ($HC(NH_2)_2I$, 99.5%, Greatcell Solar), methylammonium chlorine (CH_3NH_3Cl, 99.5%, Xi'an Polymer Light Technology Corp.), methylammonium bromide (CH_3NH_3Br, 99.5%, Greatcell Solar), 2,20,7,70-tetrakis-(N,N-di-4-methoxyphenylamino)-9,90-spirobifluorene (Spiro-OMeTAD, 99%, Xi'an Polymer Light Technology

https://doi.org/10.1007/s40820-022-00815-7

Corp.), lithium bis(trifluoromethanesulfonyl)imide (Li-TFSI, 97%, Sigma-Aldrich), 4-tert-butylpyridine (4-tBP, 98%, Sigma-Aldrich), isopropanol (IPA, 99.5%,Sigma-Aldrich), N,N-dimethylformamide (99.8%, Sigma-Aldrich), chlorobenzene (99.8%, Sigma-Aldrich), and acetonitrile (ACN, 99.95%, Sigma-Aldrich). ITO glass substrates were purchased from Shenzhen Display, China.

2.2 Materials Characterization

UV-Vis spectra were recorded on a Lambda 35 Perkin-Elmer absorption spectrometer. PL spectra were recorded using a fluorescence spectrophotometer (LS55, Perkin-Elmer). XRD patterns were obtained using a Bruker D8 Advance X-ray Diffractometer operating under Cu Kα radiation (40 kV, 40 mA) equipped with a LynxEye detector. The SEM images of the films were taken with a Zeiss Merlin field emission SEM.

2.3 Device Fabrication

2.3.1 Slot-Die Coated Devices on ITO/glass

The ITO/glass substrate was ultrasonically cleaned using detergents/H_2O, distilled water, acetone and isopropanol for 5 min sequentially. Then, dried by clean N_2 flow and treated by UV-ozone for 15 min at room temperature. For the electron transport layer, the SnO_2 nanoparticles solution that was diluted by H_2O to half of the original concentration and filtered using a 0.22 μm PVDF filter, was deposited by slot-die coating at a speed of 5 mm s^{-1} with a 1 μL cm^{-2} solution in ambient air, and followed by a post-annealing at 150 °C for 30 min. Because SnO_2 layer has been extensively used for the slot-die coating for PSCs, and an optimal thickness for perovskite devices has also been obtained [39], thus no further optimization was conducted in this work. After depositing the SnO_2 film, the perovskite layer was formed via a two-step slot-die coating deposition in ambient condition. The mixture solution of PbI_2:CsI (599.3 mg: 33.8 mg in 900 μL DMF and 100 μL DMSO) was slot-die coated at a head moving speed of 5 mm s^{-1} with a 1 μL cm^{-2} solution feed rate on the stationary SnO_2 layer, and a gap between the slot-die head and the substrate was controlled at 200 μm. The slot-die coated PbI_2:CsI films were heated at 70 °C for 3 min in ambient air. After cooling down of the PbI_2:CsI film, the mixture solution of FAI: MABr: MACl in IPA was slot-die coated at a speed of 2 mm s^{-1} with a 1 μL cm^{-2} solution feed on the PbI_2:CsI film without heating, and then post-annealed at 150 °C for 15 min in air. Subsequently, the Spiro-OMeTAD solution was drop casted or slot-die coated assisted by heating and gas blowing in ambient condition, where 1 mL Spiro-OMeTAD/chlorobenzene (90 mg mL^{-1}) solution was employed with the addition of 10 μL tBP and 45 μl Li-TFSI/ACN (170 mg mL^{-1}). Finally, 100 nm-thick Ag electrode was deposited through thermal evaporation with a mask at a pressure of 8×10^{-6} mbar, resulting in an active area of 0.1 or 1 cm^2.

2.3.2 R2R Coated Devices on Flexible ITO/PET

The R2R coating of SnO_2 was carried out by the reverse-gravure coating method, using a Mino-Labo™printer (MAHY-1310; Yasui Seiki Co.Ltd). The coating was conducted at 0.16 m min^{-1} bed speed and 16 rpm of 13 mm wide reverse-gravure roll speed to deposit the 13 mm wide continuous SnO_2 layer in the middle of the ITO/PET substrate (width: 25 mm). The coated wet SnO_2 film was dried on-line at 135 °C for 10–12 seconds on a hot plate to remove the solvent. A PbI_2:CsI solution (599.3 mg: 33.8 mg in 900 μL DMF and 100 μL DMSO) was slot-die coated on top of the SnO_2 surface (70 °C) at the feed rate of 18 μL min^{-1} and the bed speed of 0.3 m min^{-1}. The formed PbI_2:CsI film was then annealed at 70 °C assisted with N_2 blowing. The perovskite conversion was conducted by slot-die coating of a mixed solution of FAI: MABr: MACl (60 mg: 6 mg: 6 mg in 1 mL IPA) at a bed speed of 0.3 m min^{-1}, solution feed rate of 40 μL min^{-1} followed by annealing at 135 °C. Finally, Spiro-OMeTAD was slot-die coated at the bed temperature of 60 °C, bed speed of 0.3 m min^{-1} and feed rate of 40 uL min^{-1} without further annealing. The completed film was cut into 2.5 cm × 2.5 cm and 100 nm-thick Ag electrode was deposited through thermal evaporation as described in Sect. 2.3.1.

2.4 Device Measurements

Current density–voltage (*J-V*) curves of the devices were measured by a Keithley 2400 Source Meter under standard solar irradiation (AM 1.5 G, 100 mW cm^{-2}). The light intensity was calibrated using a reference cell (Hamamatsu S1133 with KG5 filter and 2.8×2.4 mm^2 of photosensitive area), which was calibrated by a certified reference cell (PV Measurements, certified by NREL) under 1000 W m^{-2} AM 1.5G illumination from a Newport LED lamp source with a ABA grade spectrum.

3 Results and Discussion

3.1 Fabrication of Perovskite Film

Figure 1 shows the fabrication schematic of PSCs using the two-step process with a device structure of ITO glass/SnO_2/Perovskite/Spiro-OMeTAD/Ag. Briefly, SnO_2 was slot-die coated on glass, followed by PbI_2:CsI film. The quality of the PbI_2:CsI film was first checked by a dipping process into the cations containing solution. Thereafter, the cation containing was also slot-die coated followed by drop casting of the hole transport layer. Finally, the hole transport layer of Spiro-OMeTAD was also slot-die coated, resulting in fully slot-die coated devices.

The quality and density of the PbI_2:CsI film strongly affect the perovskite film quality in a two-step process. Heating is a common way to dry film to reduce the effect of humidity when the wet film is deposited [40–42]. The PbI_2:CsI film tends to form a dense layer if drying dynamics is not controlled, as shown in Fig. S1a. Hence, an additional slot-die head was attached to channel N_2 blowing over the freshly slot-die coated PbI_2:CsI wet film as shown in Fig. 1. N_2 blowing enables homogenous and porous morphology formation of the PbI_2:CsI film, which provides channels facilitating cations to penetrate throughout the bulk of the PbI_2:CsI film and enable formation of a pin-hole free and fully converted homogenous perovskite film. PSCs have been demonstrated to be more efficient and stable by combining MA, FA and Cs cations [43–45]. Therefore, a similar strategy herein was employed to fabricate perovskite films. For comparison, the PbI_2:CsI films were dipped into the FAI/MABr/MACl solution at two different concentrations of 30 and 60 mg mL^{-1}, respectively. The scanning electron microscope (SEM) images of the resulting films

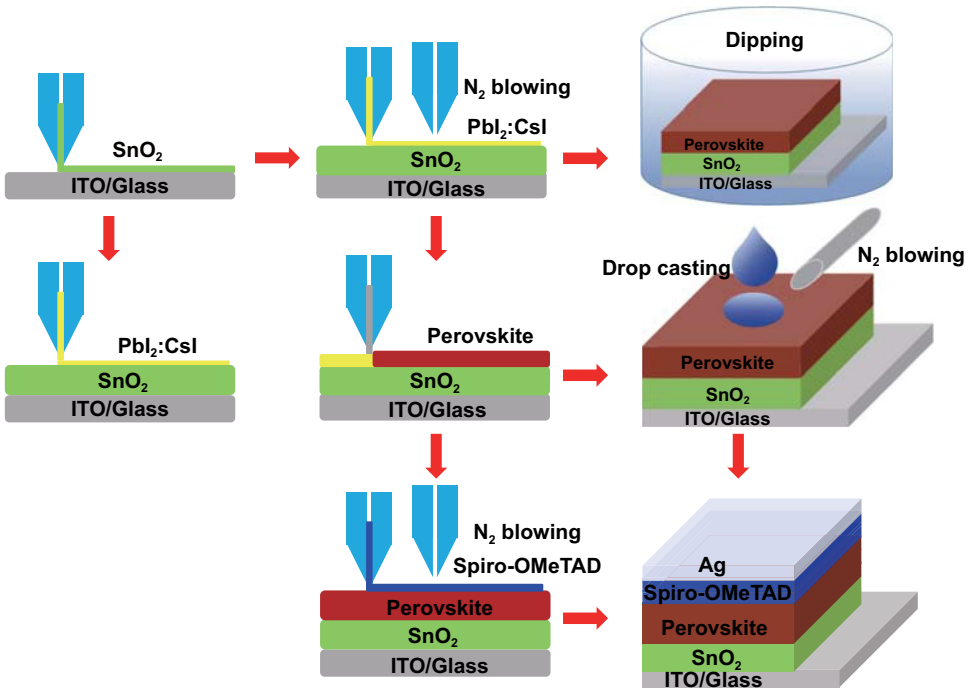

Fig. 1 Schematic of the device fabrication process

 https://doi.org/10.1007/s40820-022-00815-7

are shown in Fig. 2a, b. Clearly, the formed perovskite film at the higher concentration displays a much smoother surface than that one with the lower concentration. Hence, a 60 mg mL^{-1} FAI/MABr/MACl solution was used for further optimization and translation to slot-die coating, unless otherwise specified. One of the striking advantages of using slot-die coating compared to dipping is that much less perovskite precursor solution is required for each device. Accordingly, slot-die coating was adopted for the deposition of FAI/MABr/MACl solution. As expected, a high-quality perovskite film was achieved through this sequential process (Fig. 2c).

In the two-step fabrication process, the quality and density of PbI_2:CsI films are significant keys to facilitating the efficient conversion, leading to the desired perovskite films. The gas blowing and substrate-heating approaches are important factors that can be utilized in tandem with slot-die coating of solution to achieve desired films. Both of them can also minimize the influence of surrounding humidity to improve perovskite crystallization when being processed under an ambient environment [46]. The SnO_2-coated substrates were heated at the different bed temperatures, and the PbI_2:CsI films were deposited on top of the heated substrates. The morphologies of PbI_2:CsI films are well

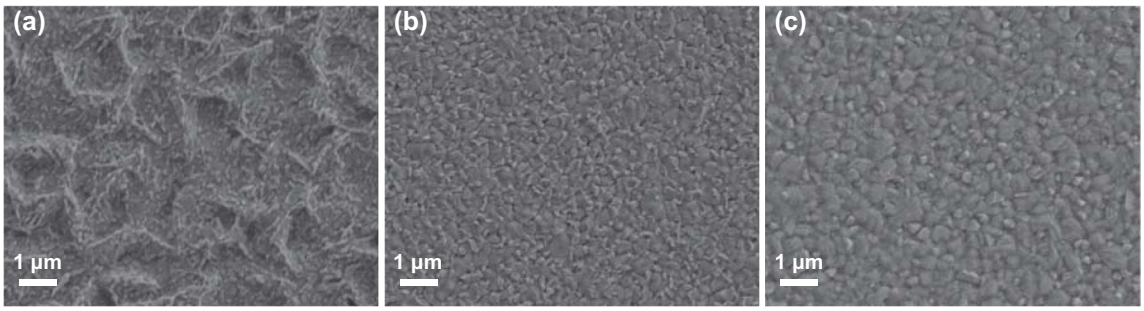

Fig. 2 **a**, **b** SEM images of perovskite films dipped in the 30 and 60 mg mL^{-1} FAI/MABr/MACl solution, respectively. **c** SEM image of perovskite film formed from slot-die coated FAI/MABr/MACl solution at 60 mg mL^{-1}

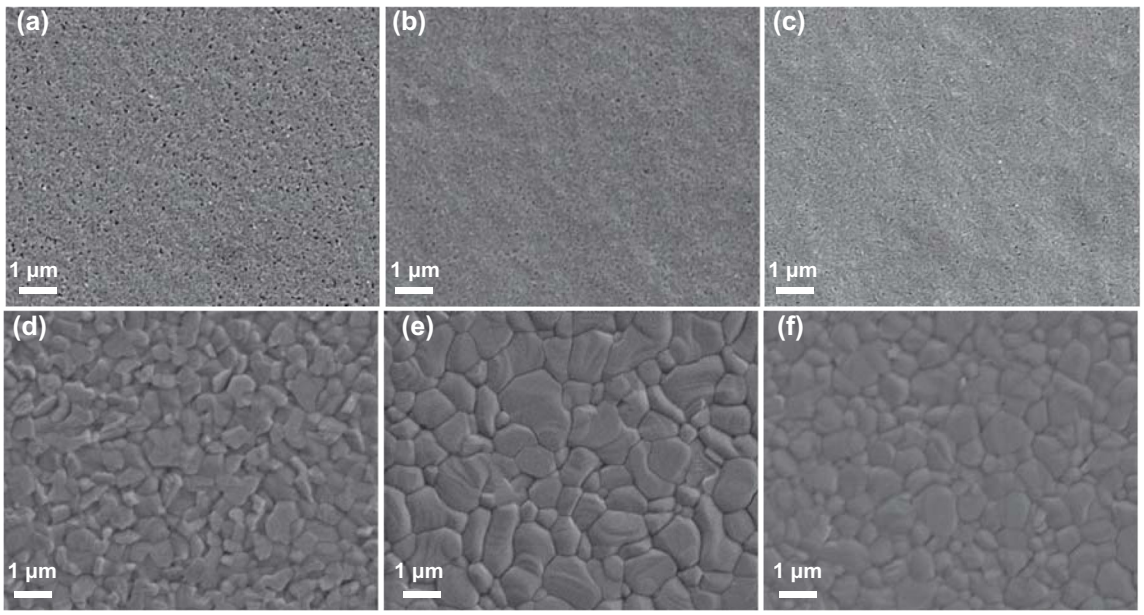

Fig. 3 **a–c** SEM images of slot-die coated PbI_2:CsI films under ambient conditions at the different bed temperatures of 60, 70, and 80 °C, respectively. **d–f** SEM images of slot-die coated perovskite films under ambient conditions at the different bed temperatures of 60, 70, and 80 °C

controlled by precise adjustment of the bed temperature and monitored by SEM. As shown in Fig. 3a-c, there are more pin-holes present within the PbI_2:CsI film when prepared at 60 °C than that at 70 °C. When the bed temperature was further increased to 80 °C, the PbI_2:CsI films tend to become compact, which is attributed to the fact that the solvent evaporates much faster at the higher temperatures, causing PbI_2:CsI crystals to precipitate quickly, forming a densely packed film. Figures 3d-f are the SEM images of perovskite films formed on the above-deposited PbI_2:CsI films at room temperature via slot-die coating of FAI/MABr/MACl solution. The perovskite grain size is summarized by analyzing the size of 150 grains through Nano Measurer software, as shown in Fig. S2. The grain size increases initially along with the bed temperature changing from 60 to 70 °C, and then decreases when the bed temperature reached 80 °C. This trend can be attributed to the supersaturation of PbI_2 crystals at high bed temperature, leading to the excessive incomplete converted PbI_2, which will be discussed in detail below. The optimal number of pores would provide enough space for FAI/MABr/MACl to diffuse into PbI_2:CsI films, enabling complete conversion to perovskite. On the contrary, too densely packed PbI_2:CsI film hinders the solution diffusion into the PbI_2:CsI bulk film, inhibiting efficient interaction between PbI_2:CsI and FAI/MABr/MACl, causing incomplete conversion to perovskite and negatively impacting device performance. Therefore, the quality of PbI_2:CsI films controlled by bed temperature exhibits considerable effects on the fabrication of high-quality perovskite films. Thus, the results suggest that an optimal porous morphology of the PbI_2:CsI film is critical to form smooth, homogeneous, fully converted perovskite films with large grains, while a dense PbI_2:CsI layer leads to the incomplete conversion into perovskite [47].

3.2 Characterization of Perovskite Film

Figure 4a shows UV–vis absorption spectra of the perovskite films fabricated at different bed temperatures using a standard detector. All the perovskite films exhibit similar

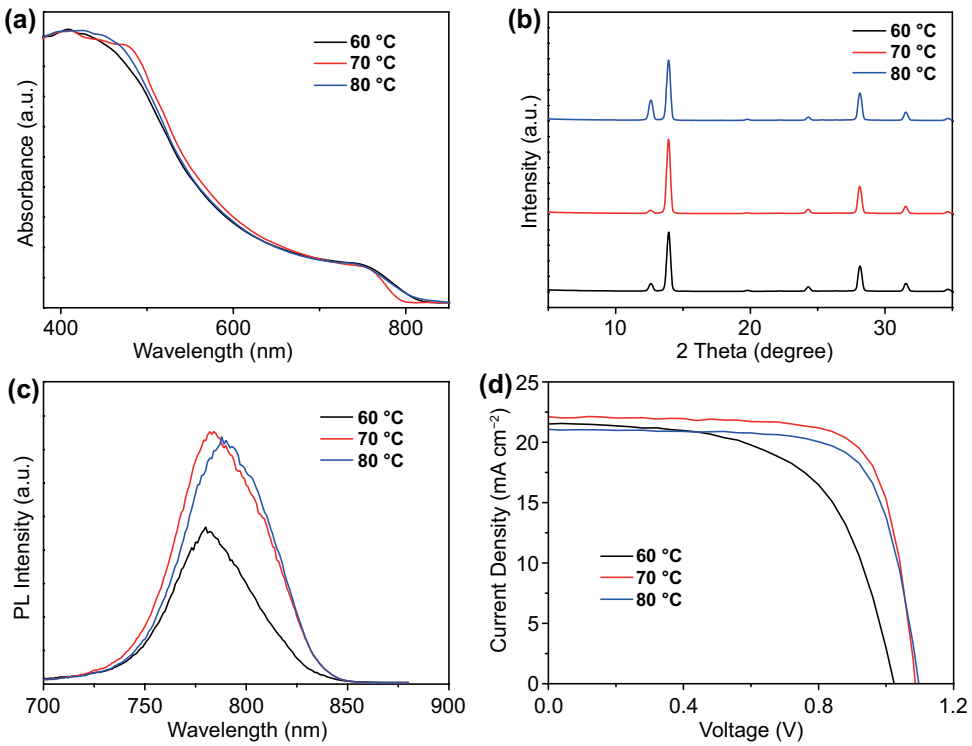

Fig. 4 **a** Absorbance spectra, **b** XRD patterns, **c** photoluminescence and **d** *J*–*V* curves of perovskite films prepared using the PbI_2:CsI films fabricated on the different bed temperatures

https://doi.org/10.1007/s40820-022-00815-7

absorption as previously reported. The XRD results are displayed in Fig. 4b. When the bed temperature increased to 80 °C, a small peak at $2\theta = 12.7°$ distinctly appeared in the XRD patterns. This typical peak is ascribed to the unreacted excessive PbI_2 crystals that primarily reside at the bottom of perovskite film. For investigating the effect of bed temperature on photogenerated charge carriers of the perovskite film, the steady-state photoluminescence (PL) spectra were measured on perovskite films prepared on glass substrate using the same two-step process (Fig. 4c). The perovskite film fabricated at 70 °C presents the highest PL intensity, implying that the nonradiative recombination of perovskite film was significantly suppressed at this bed temperature. The PL peak of perovskite film fabricated at 80 °C has a small redshift, which indicates a higher trap density in perovskite film [48]. Therefore, the increased recombination loss and reduced charge collection of the perovskite film prepared at 80 °C will have a negative influence on the solar cell performance.

The *J-V* curves and performance parameters of PSC devices fabricated from the above perovskite films prepared at different bed temperatures are shown and summarized in Fig. 4d and Table 1, respectively. Slot-die coating was used for the deposition of SnO_2 and perovskite layers, except that Spiro-OMeTAD hole transport layer was coated by drop-casting. The short-circuit current (J_{sc}) increased when the bed temperature increased from 60 to 70 °C. On the contrary, the J_{sc} slightly decreased with increasing the bed temperature to 80 °C. The highest J_{sc} of 22.11 mA cm^{-2} was achieved at the optimized bed temperature of 70 °C. Meanwhile, the fill factor (*FF*) was also improved to 75.2%, resulting in the final PCE of 17.96%. The achieved device results comply with the previous result analysis from SEM, PL and XRD. Conspicuously, a suitable bed temperature is crucial in determining PbI_2:CsI film morphology and in turn final device performance. The bed temperature at 80 °C accelerates solvent evaporation, resulting in the unavoidable high density of PbI_2:CsI film, which causes the incomplete conversion of PbI_2:CsI to perovskite. At this point, slot-die coating as an effective way to deposit PbI_2:CsI and perovskite film at the certain temperatures range has been demonstrated. This setup is believed to be readily transferred to the R2R continuous process.

3.3 Photovoltaic Performance of Fully Slot-Die Coated PSCs

Notwithstanding the impressive performance parameters were obtained from the slot-die coated perovskite layer on the glass substrate, the industrial compatible process requires all layers to be fabricated with scalable deposition strategies. Figure 5a shows a SEM cross-section of the PSCs, in which all layer but the electrodes, namely SnO_2, perovskite layer and Spiro-OMeTAD layer, were slot-die coated. The thickness of the perovskite film reaches about 650 nm. The *J-V* curves of the best performance of PSCs are shown in Fig. 5b. The champion cell exhibits an open-circuit voltage (V_{oc}) of 1.08 V, a J_{sc} of 22.09 mA cm^{-2}, an *FF* of 76.01%, and a PCE of 18.13% in a reverse scan. A steady-state PCE of 17.57% was obtained (Fig. 5c). Extending slot-die coating to large-area fabrication, 1 cm^2 device was fabricated via the same process (Fig. S3). *J-V* curves of 8 PSC devices are presented in Fig. 5d, and the corresponding PCEs are shown in the inset. The champion 1 cm^2 device shows a PCE of 15.10%, which demonstrates that large-area PSCs could be effectively fabricated by slot-die coating in ambient conditions.

3.4 Fully R2R Processed PSCs

The slot-die coating was then transferred to R2R coating process (Fig. 6a). The flexible ITO/PET substrate was continuously moved from an unwind roller, passing the coating head and dryer, and finally to the rewind roller. When each

Table 1 Average values of photovoltaic parameters obtained from *J–V* measurements for PSCs derived from PbI_2:CsI prepared by slot-die coating under ambient conditions at the different bed temperature

Temperature (°C)	V_{oc} (V)	J_{sc} (mA cm^{-2})	*FF* (%)	*PCE* (%)	*PCE* (Max)
60	1.05 ± 0.04	20.90 ± 0.72	58.42 ± 3.39	12.90 ± 0.94	13.98
70	1.08 ± 0.02	22.09 ± 0.35	74.30 ± 1.12	17.80 ± 0.13	17.96
80	1.07 ± 0.02	21.29 ± 0.32	71.22 ± 2.38	16.28 ± 0.55	16.86

The performance parameters are the average values of 8 devices

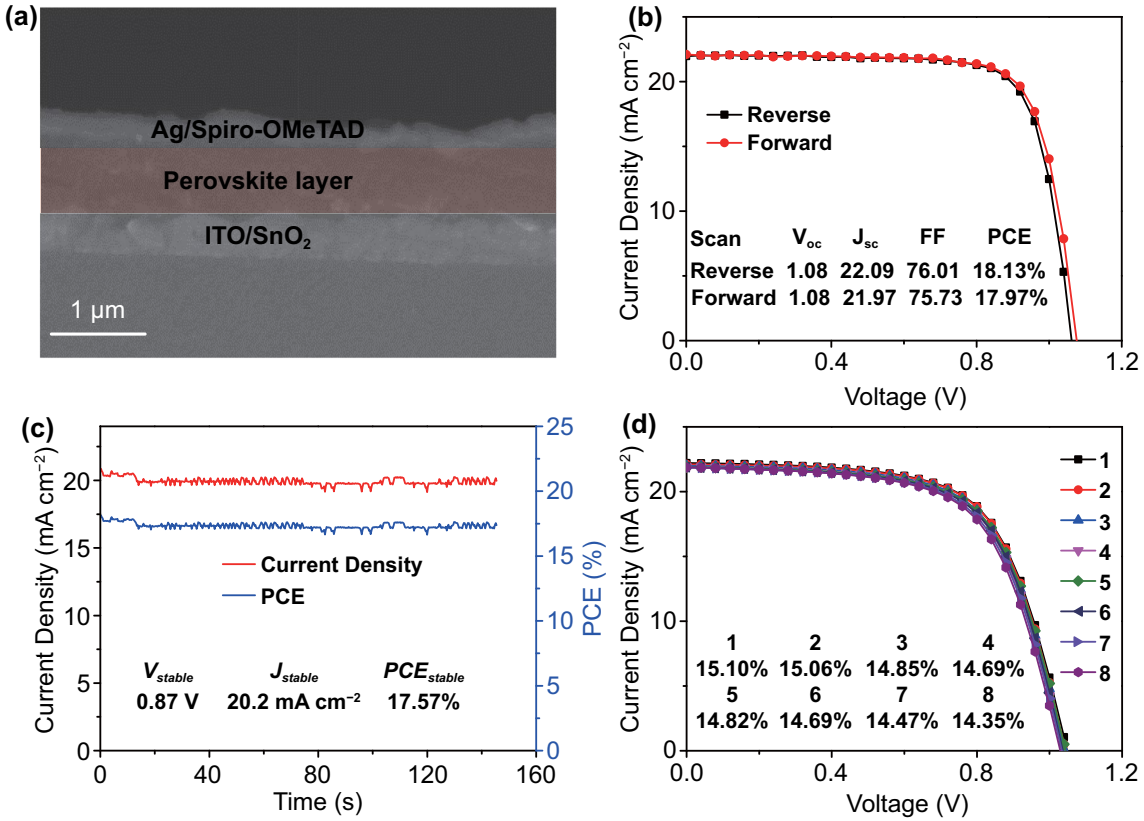

Fig. 5 **a** SEM cross-sectional image for a fully slot-die coated PSC except for the electrode. **b** *J*–*V* curves of the champion cell under reverse and forward scan. **c** Steady-state PCE of the champion cell. **d** *J*–*V* curves of 8 PSCs with 1 cm^2 area fabricated by fully slot-die coating except for the electrode

coating run was completed, the substrate was collected on the rewind roller. To start, a thin SnO_2 film was first coated by micro-gravure printing, followed by slot-die coated of the PbI_2:CsI layer which was dried by N_2 blowing, and finally converted to the perovskite film by slot-die coating of FAI/MABr/MACl solution. The detailed R2R coating conditions are described in the experimental session. As shown in Fig. 6a, hot plate-1 is employed to heat the wet film during the coating process as a bed temperature, and the hot plate-2 is used to anneal the dried film. The best performance of PSCs using the R2R coating process present a V_{oc} of 1.00 V, a J_{sc} of 21.45 mA cm^{-2}, an *FF* of 60.59, and a PCE of 13.00% in a reverse scan (Fig. 6b and Table 2). As shown in Table 2, the hysteresis behavior of R2R coated devices is worse than the slot-die coated ITO/glass substrates. Normally, it is very difficult to control morphology and interface properties of PSCs on flexible substrate using R2R coating process, which would result in more traps in thin film and interface. The trap assisted charge recombination may occur at the interface between the SnO_2 layer and the perovskite layer. Thus, both ion movement and traps enhance the hysteresis behavior [49–51]. Figure 6c presents the statistical distribution of the PCEs based on 25 PSCs, and the average PCE is about 11.30%.

4 Conclusions

In summary, high-quality perovskite films are successfully prepared in ambient conditions via slot-die coating on ITO/glass substrates and continuous R2R coating on flexible substrates. The influence of bed temperature on the morphology of PbI_2:CsI film during the coating was fully investigated. PL

https://doi.org/10.1007/s40820-022-00815-7

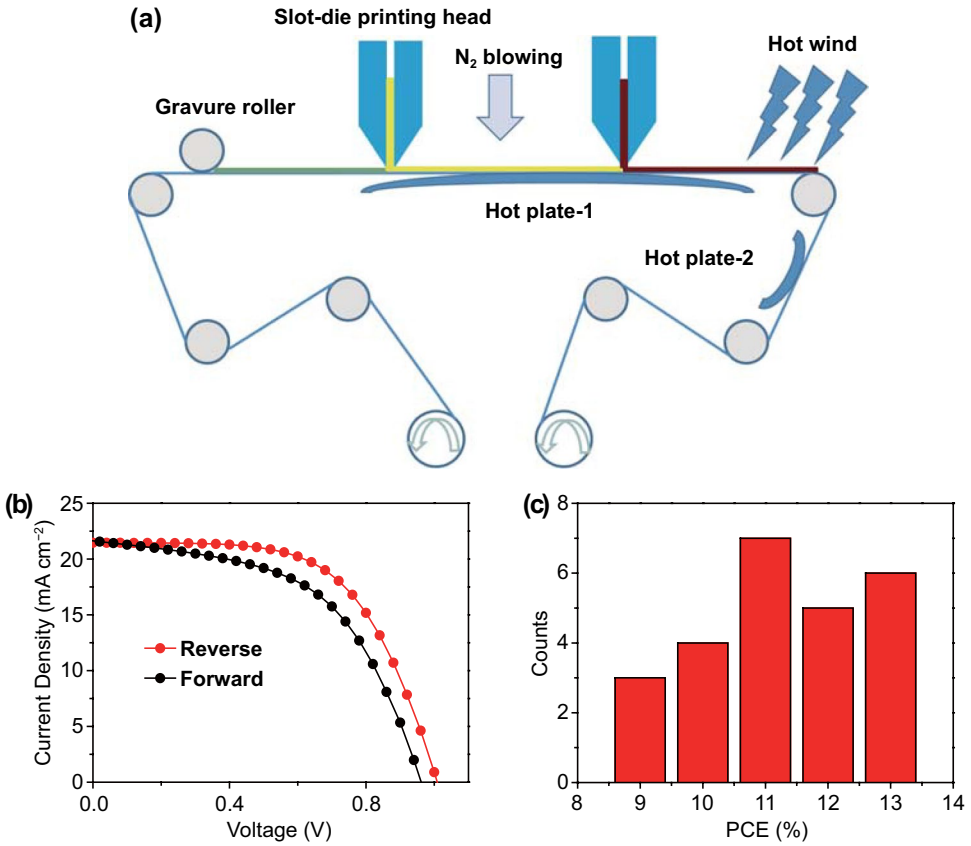

Fig. 6 **a** R2R processing set-up for continuous preparation of PSCs. **b** *J–V* curves for the champion device fabricated by R2R coating. **c** The distribution of PCEs obtained from R2R processed 25 devices

Table 2 The performance parameters of the champion PSCs prepared by slot-die coating were measured under reverse and forward scan directions

Method	Scan direction	V_{oc} (V)	J_{sc} (mA cm^{-2})	*FF* (%)	*PCE* (%)
Slot-die on glass	Reverse	1.08	22.09	76.01	18.13
Slot-die on glass	Forward	1.08	21.97	75.73	17.97
R2R coating	Reverse	1.00	21.45	60.59	13.00
R2R coating	Forward	0.98	21.56	52.51	11.09

and XRD results support the explanation of variable device performances in solar cells when prepared at the different temperatures. Planar n-i-p PSCs with a PCE of 18.13% was achieved by fully slot-die coating. A PCE of 15.10% was achieved for PSCs with an area of 1 cm^2. Furthermore, the flexible PSC with a PCE of 13.00% was obtained on ITO/PET substrate by the R2R coating process, which is currently one of the highest perovskite performances for fully R2R fabricated PSCs in ambient air. These results will undoubtedly help further pave the way in improving the performance of the large scale PSCs in ambient conditions and catalyse the pursuit towards low cost mass production in the future.

Acknowledgements The authors acknowledge support from the Australian Centre for Advanced Photovoltaics (ACAP) program funded by the Australian Government through the Australian Renewable Energy Agency (ARENA), the Devices & Engineered System Program of CSIRO Manufacturing. HL and JY acknowledge support from the National Natural Science Foundation of China (Grant No. 52173192) and the National Key Research and Development Program of China (Grant No. 2017YFA0206600). HL also acknowledges the support from the Key Innovation Project of Graduate of Central South University (Grant No. 2018ZZTS106) and China Scholarship Council program.

Funding Open access funding provided by Shanghai Jiao Tong University.

Supplementary Information The online version contains supplementary material available at https://doi.org/10.1007/s40820-022-00815-7.

References

1. A. Kojima, K. Teshima, Y. Shirai, T. Miyasaka, Organometal halide perovskites as visible-light sensitizers for photovoltaic cells. J. Am. Chem. Soc. **131**(17), 6050–6051 (2009). https://doi.org/10.1021/ja809598r
2. https://www.nrel.gov/pv/cell-efficiency.html
3. S.P. Dunfield, L. Bills, F. Zhang, J.M. Luther, K. Zhu et al., From defects to degradation: a mechanistic understanding of degradation in perovskite solar cell devices and modules. Adv. Energy Mater. **10**(26), 1904054 (2020). https://doi.org/10.1002/aenm.201904054
4. Z.H. Dai, S. Yadavalli, M. Chen, Y. Qi, N.P. Padture, Interfacial toughening with self-assembled monolayers enhances perovskite solar cell reliability. Science **372**(6542), 618–622 (2021). https://doi.org/10.1126/science.abf5602
5. S.W. Song, S.J. Yang, W. Choi, H. Lee, W. Sung et al., Molecular engineering of organic spacer cations for efficient and stable formamidinium perovskite solar cell. Adv. Energy Mater. **10**(42), 2001759 (2020). https://doi.org/10.1002/aenm.202001759
6. H.Y. Li, C.T. Zuo, A.D. Scully, D. Angmo, J.L. Yang et al., Recent progress towards roll-to-roll manufacturing of perovskite solar cells using slot-die processing. Flex. Print. Elecron. **5**, 014006 (2020). https://doi.org/10.1088/2058-8585/ab639e
7. K.J. Liao, C.B. Li, L.S. Xie, Y. Yuan, S.R. Wang et al., Hot-casting large-grain perovskite film for efficient solar cells: film formation and device performance. Nano-Micro Lett. **12**, 156 (2020). https://doi.org/10.1007/s40820-020-00494-2
8. S. Ngqoloda, C.J. Arendse, T.F. Muller, P.F. Miceli, S. Guha et al., Air-stable hybrid perovskite solar cell by sequential vapor deposition in a single reactor. ACS Appl. Energy Mater. **3**(3), 2350–2359 (2020). https://doi.org/10.1021/acsaem.9b01925
9. D.Q. Bi, X. Li, J.V. Milic, D.J. Kubicki, N. Pellet et al., Multifunctional molecular modulators for perovskite solar cells with over 20% efficiency and high operational stability. Nat. Commun. **9**, 4482 (2018). https://doi.org/10.1038/s41467-018-06709-w
10. H. Min, M. Kim, S.U. Lee, H. Kim, G. Kim et al., Efficient, stable solar cells by using inherent bandgap of α-phase formamidinium lead iodide. Science **336**(6466), 749–753 (2019). https://doi.org/10.1126/science.aay7044
11. M. Kim, G.H. Kim, T.K. Lee, I.W. Choi, Y. Jo et al., Methylammonium chloride induces intermediate phase stabilization for efficient perovskite solar cells. Joule **3**(9), 2179–2192 (2019). https://doi.org/10.1016/j.joule.2019.06.014
12. W.J. Zhao, J. Xu, K. He, Y. Cai, S.M. Yang et al., A special additive enables all cations and anions passivation for stable perovskite solar cells with efficiency over 23%. Nano-Micro Lett. **13**, 169 (2021). https://doi.org/10.1007/s40820-021-00688-2
13. H. Ren, S.D. Yu, L.F. Chao, Y.D. Xia, Y.H. Sun et al., Efficient and stable ruddlesden-popper perovskite solar cell with tailored interlayer molecular interaction. Nat. Photonics **14**, 154–163 (2020). https://doi.org/10.1038/s41566-019-0572-6
14. S. Ghosh, T. Singh, Role of ionic liquids in organic-inorganic metal halide perovskite solar cells efficiency and stability. Nano Energy **63**, 103828 (2019). https://doi.org/10.1016/j.nanoen.2019.06.024
15. K.N. Noel, S.N. Habisreutinger, B. Wenger, M.T. Klug, M.T. Horantner et al., A low viscosity, low boiling point, clean solvent system for the rapid crystallisation of highly specular perovskite films. Energy Environ. Sci. **10**(1), 145–152 (2017). https://doi.org/10.1039/c6ee02373h
16. Z.Q. Lin, H.J. Lian, B. Ge, Z.R. Zhou, H.Y. Yuan et al., Mediating the local oxygen-bridge interactions of oxysalt/perovskite interface for defect passivation of perovskite photovoltaics. Nano-Micro Lett. **13**, 177 (2021). https://doi.org/10.1007/s40820-021-00683-7
17. J. Xiong, B.C. Yang, C.H. Cao, R.S. Wu, Y.L. Huang et al., Interface degradation of perovskite solar cells and its modification using an annealing-free TiO_2 NPs layer. Org. Electron. **30**, 30–35 (2016). https://doi.org/10.1016/j.orgel.2015.12.010
18. I.A. Howard, T. Abzieher, I.M. Hossain, H. Eggers, F. Schackmar et al., Coated and printed perovskites for photovoltaic

applications. Adv. Mater. **31**(26), 1806702 (2019). https://doi.org/10.1002/adma.201806702

19. J.W. Lee, D.K. Lee, D.N. Jeong, N.G. Park, Control of crystal growth toward scalable fabrication of perovskite solar cells. Adv. Funct. Mater. **29**(47), 1807047 (2019). https://doi.org/10.1002/adfm.201807047
20. F. Huang, M.J. Li, P. Siffalovic, G.Z. Cao, J.J. Tian, From scalable solution fabrication of perovskite films towards commercialization of solar cells. Energy Environ. Sci. **12**(2), 518–549 (2019). https://doi.org/10.1039/c8ee03025a
21. M.L. Xie, H. Lu, L.P. Zhang, J. Wang, Q. Luo et al., Fully solution-processed semi-transparent perovskite solar cells with ink-jet printed silver nanowires top electrode. Sol. RRL **2**(2), 1700184 (2018). https://doi.org/10.1002/solr.201700184
22. J.H. Chang, K. Liu, S.Y. Lin, Y.B. Yuan, C.H. Zhou et al., Solution-processed perovskite solar cells. J. Cent. South Univ. **27**, 1104–1133 (2020). https://doi.org/10.1007/s11771-020-4353-7
23. D. Angmo, G. Deluca, A.D. Scully, A.S.R. Chesman, A. Seeber et al., A lab-to-fab study toward roll-to-roll fabrication of reproducible perovskite solar cells under ambient room conditions. Cell Rep. Phys. Sci. **2**(1), 100293 (2021). https://doi.org/10.1016/j.xcrp.2020.100293
24. F.Z. Li, Y. Zhang, K.J. Jiang, C.S. Zhang, J.H. Huang et al., A novel strategy for scalable high-efficiency planar perovskite solar cells with new precursors and cation displacement approach. Adv. Mater. **30**(44), 1804454 (2018). https://doi.org/10.1002/adma.201804454
25. W.Q. Wu, P.N. Rudd, Q. Wang, Z.B. Yang, J.S. Huang, Blading phase-pure formamidinium-alloyed perovskites for high-efficiency solar cells with low photovoltage deficit and improved stability. Adv. Mater. **32**(28), 2000995 (2020). https://doi.org/10.1002/adma.202000995
26. C.T. Zuo, D. Vak, D. Angmo, L.M. Ding, M. Gao, One-step roll-to-roll air processed high efficiency perovskite solar cells. Nano Energy **46**, 185–192 (2018). https://doi.org/10.1016/j.nanoen.2018.01.037
27. C.D. Gong, S.C. Tong, K.Q. Huang, H.Y. Li, H. Huang et al., Flexible planar heterojunction perovskite solar cells fabricated via sequential roll-to-roll microgravure printing and slot-die coating deposition. Sol. RRL **4**(2), 1900304 (2019). https://doi.org/10.1002/solr.201900204
28. J.E. Kim, S.S. Kim, C.T. Zuo, M. Gao, D. Vak et al., Humidity-tolerant roll-to-roll fabrication of perovskite solar cells via polymer-additive-assisted hot slot die deposition. Adv. Funct. Mater. **29**(26), 1809194 (2019). https://doi.org/10.1002/adfm.201809194
29. Y.J. Heo, J.E. Kim, H. Weerasinhe, D. Angmo, T.S. Qin et al., Printing-friendly sequential deposition via intra-additive approach for rollto-roll process of perovskite solar cells. Nano Energy **41**, 443–451 (2017). https://doi.org/10.1016/j.nanoen.2017.09.051
30. Y.Y. Kim, E.Y. Park, T.Y. Yang, J.H. Noh, T.J. Shin et al., Fast two-step deposition of perovskite via mediator extraction treatment for large-area, high performance perovskite solar cells. J. Mater. Chem. A **6**(26), 12447–12454 (2018). https://doi.org/10.1039/c8ta02868k
31. Y. Li, L. Ji, R.G. Liu, A review on morphology engineering for highly efficient and stable hybrid perovskite solar cells. J. Mater. Chem. A **6**(27), 12842–12875 (2018). https://doi.org/10.1039/c8ta04120b
32. Y.Y. Kim, T.Y. Yang, R. Suhonen, M. Valimaki, T. Maaninen et al., Gravure-printed flexible perovskite solar cells: toward roll-to-roll manufacturing. Adv. Sci. **6**(7), 1802094 (2019). https://doi.org/10.1002/advs.201802094
33. Y.Y. Kim, T.Y. Yang, R. Suhonen, A. Kemppainen, K. Hwang et al., Roll-to-roll gravure-printed flexible perovskite solar cells using eco-friendly antisolvent bathing with wide processing window. Nat. Comm. **11**, 5146 (2020). https://doi.org/10.1038/s41467-020-18940-5
34. D. Burkitt, R. Patidar, P. Greenwood, K. Hooper, J. Mcgettric et al., Roll-to-roll slot-die coated P-I-N perovskite solar cells using acetonitrile based singly step perovskite solvent system. Sustain. Energy Fuels **4**(7), 3340–3351 (2020). https://doi.org/10.1039/D0SE00460J
35. M. Othman, F. Zheng, A. Seeber, A.S.R. Chesman, A.D. Scully et al., Millimeter-sized clusters of triple cation perovskite enables highly efficient and reproducible roll-to-roll fabricated inverted perovskite solar cells. Adv. Funct. Mater. (2021). https://doi.org/10.1002/adfm.202110700
36. J. Burschka, N. Pellet, S.J. Moon, B.R. Humphry, P. Gao et al., Sequential deposition as a route to high-performance perovskite-sensitized solar cells. Nature **499**, 316–319 (2013). https://doi.org/10.1038/nature12340
37. C.H. Wang, C.J. Zhang, S.T. Wang, G. Liu, H.Y. Xia et al., Low-temperature processed, efficient, and highly reproducible cesium-doped triple cation perovskite planar heterojunction solar cells. Sol. RRL **2**(2), 1700209 (2018). https://doi.org/10.1002/solr.201700209
38. K.Q. Huang, Y.Y. Peng, Y.X. Gao, J. Shi, H.Y. Li et al., High-performance flexible perovskite solar cells via precise control of electron transport layer. Adv. Energy Mater. **9**(44), 1901419 (2019). https://doi.org/10.1002/aenm.201901419
39. T.L. Bu, J. Li, F. Zheng, W.J. Chen, X.M. Wen et al., Universal passivation strategy to slot-die printed SnO_2 for hysteresis-free efficient flexible perovskite solar module. Nat. Commun. **9**, 4609 (2018). https://doi.org/10.1038/s41467-018-07099-9
40. C.T. Zuo, A. Scully, D. Yak, W.L. Tan, X.C. Jiao et al., Self-assembled 2D perovskite layers for efficient printable solar cells. Adv. Energy Mater. **9**(4), 1803258 (2019). https://doi.org/10.1002/aenm.201803258
41. H. Wu, C.J. Zhang, K.X. Ding, L.J. Wang, Y.L. Gao et al., Efficient planar heterojunction perovskite solar cells fabricated by in-situ thermal-annealing doctor blading in ambient condition. Org. Electron. **45**, 302–307 (2017). https://doi.org/10.1016/j.orgel.2017.03.017
42. C.C. Boyd, R. Cheacharoen, K.A. Bush, R. Prasanna, T. Leijtens et al., Barrier design to prevent metal-induced degradation and improve thermal stability in perovskite solar cells. ACS Energy Lett. **3**(7), 1772–1778 (2018). https://doi.org/10.1021/acsenergylett.8b00926

43. F.M. Li, Z.T. Shen, Y.J. Weng, Q. Lou, C. Chen et al., Novel electron transport layer material for perovskite solar cells with over 22% efficiency and long-term stability. Adv. Funct. Mater. **30**(45), 2004933 (2020). https://doi.org/10.1002/adfm.202004933
44. K. Ma, H.R. Atapattu, Q.C. Zhao, Y. Gao, B.P. Finkenauer et al., Multifunctional conjugated ligand engineering for stable and efficient perovskite solar cells. Adv. Mater. **33**(32), 2100791 (2021). https://doi.org/10.1002/adma.202100791
45. M.M. Tavakoli, M. Saliba, P. Yadav, P. Holzhey, A. Hagfeldt et al., Synergistic crystal and interface engineering for efficient and stable perovskite photovoltaics. Adv. Energy Mater. **9**(1), 1802646 (2019). https://doi.org/10.1002/aenm.201802646
46. Q.D. Tai, P. You, H.Q. Sang, Z.K. Liu, C.L. Hu et al., Efficient and stable perovskite solar cells prepared in ambient air irrespective of the humidity. Nat. Commun. **7**, 11105 (2016). https://doi.org/10.1038/ncomms11105
47. T.J. Jacobsson, J.P. Correa, E.H. Anaraki, B. Philippe, S.D. Stranks et al., Unreacted PbI_2 as a double-edged sword for enhancing the performance of perovskite solar cells. J. Am. Chem. Soc. **138**(32), 10331–10343 (2016). https://doi.org/10.1021/jacs.6b06320
48. J.J. Tian, Q.F. Xue, X.F. Tang, Y.X. Chen, N. Li et al., Dual interfacial design for efficient $CsPbI_2Br$ perovskite solar cells with improved photostability. Adv. Mater. **31**(23), 1901152 (2019). https://doi.org/10.1002/adma.201901152
49. P.Y. Liu, W. Wang, S.M. Liu, H.G. Yang, Z.P. Shao, Fundamental understanding of photocurrent hysteresis in perovskite solar cells. Adv. Energy Mater. **9**(13), 1803017 (2019). https://doi.org/10.1002/aenm.201803017
50. W. Tress, J.P.C. Baena, M. Saliba, A. Abate, M. Graetzel, Inverted current-voltage hysteresis in mixed perovskite solar cells: polarization, energy barriers, and defect recombination. Adv. Energy Mater. **6**(19), 1600396 (2016). https://doi.org/10.1002/aenm.201600396
51. M.F. Ayguler, A.G. Hugnagel, P. Rieder, M. Wussler, W. Jaegermann, Influence of fermi level alignment with tin oxide on the hysteresis of perovskite solar cells. ACS Appl. Mater. Interfaces **10**(14), 11414–11419 (2018). https://doi.org/10.1021/acsami.8b00990

 https://doi.org/10.1007/s40820-022-00815-7